

Green Chemistry

Accepted Manuscript



This is an *Accepted Manuscript*, which has been through the Royal Society of Chemistry peer review process and has been accepted for publication.

Accepted Manuscripts are published online shortly after acceptance, before technical editing, formatting and proof reading. Using this free service, authors can make their results available to the community, in citable form, before we publish the edited article. We will replace this *Accepted Manuscript* with the edited and formatted *Advance Article* as soon as it is available.

You can find more information about *Accepted Manuscripts* in the [Information for Authors](#).

Please note that technical editing may introduce minor changes to the text and/or graphics, which may alter content. The journal's standard [Terms & Conditions](#) and the [Ethical guidelines](#) still apply. In no event shall the Royal Society of Chemistry be held responsible for any errors or omissions in this *Accepted Manuscript* or any consequences arising from the use of any information it contains.



www.rsc.org/greenchem

Upgrading biomass pyrolysis vapors over β -zeolites: role of Silica-to-Alumina ratio

Calvin Mukarakate,^{*a} Michael Watson,^b Jeroen ten Dam,^b Xavier Baucherel,^b Sridhar Budhi,^{a,c} Matthew Yung,^a Haoxi Ben,^a Kristiina Iisa,^a Robert M. Baldwin,^a and Mark R. Nimlos^a

^aNational Bioenergy Center, National Renewable Energy Laboratory, 15013 Denver West Parkway, Golden, CO 80401-3393

^bJohnson Matthey Technology Centre, PO Box 1, Belasis Avenue, Billingham, Cleveland, TS23 1LB, UK

^cDepartment of Chemistry and Geochemistry, Colorado School of Mines, Golden, CO 80401

Abstract

The conversion of biomass primary pyrolysis vapors over several β -zeolites with silica-to-alumina ratios (SAR) varying from 21 to 250 was carried out in a flow microreactor to investigate the effect of number of acid sites on product speciation and deactivation of the catalyst. Experiments were conducted using a horizontal fixed bed semi-batch reactor in which up to 40 discrete 50 mg batches of biomass were pyrolyzed and the vapors upgraded over 0.5 g of the catalyst. Products were measured with a molecular beam mass spectrometer (MBMS). These studies were complemented using a tandem micropyrolyzer connected to a GCMS (py-GCMS) for speciation and quantifying the products. In the py-GCMS experiments, several 0.5 mg loads of pine were pyrolyzed sequentially and the vapors upgraded over 4 mg of catalyst. In all of these experiments, real-time measurements of the products formed were conducted as the catalyst aged and deactivated during upgrading. The results from these experiments showed that: 1) fresh catalyst for β -zeolites with lower SAR (more acid sites) produced primarily aromatic hydrocarbons and olefins with no detectable oxygen-containing species; 2) a suite of oxygenated products was observed from fresh catalysts with high SAR (few acid sites), indicating that 0.5 g of these catalyst materials did not have sufficient acid sites to deoxygenate vapors produced from pyrolysis of 50 mg of pine. This suite of oxygen containing products consisted of furans, phenol and cresols. The amount of coke deposited on each catalyst and the yield of aromatic hydrocarbons increased with the number of acid sites. However, normalizing the results by the amount of biomass pyrolyzed resulted in the same amount of coke and hydrocarbon yields.

Corresponding author

E-mail: calvin.mukarakate@nrel.gov

1. Introduction

The conversion of biomass into liquid transportation fuels has attracted significant attention because of depleting fossil fuel reserves and environmental concerns resulting from the use of fossil fuels. Biomass is a renewable resource, which is abundant world-wide and can potentially be exploited to produce transportation fuels that are less damaging to the environment. This renewable resource consists of cellulose (40-50%), hemicellulose (25-35%), and lignin (16-33%) biopolymers in addition to smaller quantities of inorganic materials such as silica and alkali and alkaline earth metals (calcium and potassium). Fast pyrolysis is an attractive thermochemical technology for converting biomass into precursors for hydrocarbon fuels because it produces up to 75 wt% bio-oil,¹ which can be upgraded to feedstocks and/or blendstocks for further refining to finished fuels. Bio-oil that has not been upgraded has limited applications because of the presence of oxygen-containing functional groups, derived from cellulose, hemicellulose and lignin, which gives rise to high acidity, high viscosity, low heating value, immiscibility with hydrocarbons and ageing during storage.¹⁻⁶ Ex-situ catalytic vapor phase upgrading is a promising approach for improving the properties of bio-oil. This process occurs when the primary pyrolysis vapors are passed over catalysts at elevated temperature and near-ambient pressure before condensation. The goal of this process is to reject oxygen and produce a bio-oil with improved properties for subsequent downstream conversion to hydrocarbons.

Several forms of zeolites (ZSM-5, Y-zeolite, mordenite, ferrierite and β -zeolite) have been investigated previously for upgrading of biomass pyrolysis vapors to produce aromatic hydrocarbons.⁷⁻³⁵ These studies reported low yields of hydrocarbons, high light gas production, and high coking rates resulting in rapid deactivation of the catalyst, all of which represent significant technical and economic barriers towards commercial deployment of bio-oil in the transportation fuels industry.

In order to improve the yield of upgraded products and reduce coke formation previous researchers investigated the effect of zeolite structure and properties on upgrading of bio-oils and vapors from biomass pyrolysis. For example, zeolites with different pore sizes and pore structures were investigated by Vitolo et al.,^{30, 31} who proposed that the active sites were Brønsted acid sites, with the upgrading chemistry acting through a carbonium ion mechanism to promote deoxygenation of the bio-oil as well as cracking, oligomerization, alkylation, isomerization, cyclization and aromatization. Carlson et al.,³⁶ tested five catalysts for upgrading biomass pyrolysis products and reported that Brønsted acid sites were necessary for production of aromatics. They also reported that Y-zeolite, β -zeolite and silica-alumina catalysts were best for producing small aromatics, such as benzene and toluene, whereas HZSM-5 and silicalite catalysts were optimal for producing larger aromatics such as naphthalene and indane.

Putun et al.,²⁵ upgraded biomass vapors using natural zeolite, ZSM-5 and HY zeolites. They found that zeolites with larger pore sizes and lower silica-to-alumina ratios (SAR) had higher activities, which caused coking, tar formation and low oil yields.

Ben et al.,³⁷ examined the influence of SAR of ZSM-5 on the properties of lignin pyrolysis products. They found that HZSM-5 zeolites with a higher SAR were more effective at the elimination of methoxyl groups, cleaving ether and aliphatic C–C bonds, and dehydration of aliphatic hydroxyl groups during pyrolysis. Ben et al.,³⁸ also tested five different zeolites (HZSM-5, faujasite, β -zeolite, ferrierite, and mordenite) and found that the bio-oil obtained using β -zeolite contained 80% less methoxyl groups, and the average molecular weight of upgraded pyrolysis oil decreased by more than 60% compared to non-catalytic pyrolysis. The final product had a molecular weight that was close to the gasoline range (80-120 g/mol).

Aho et al.,³⁹ investigated the influence of different structures of acidic zeolites (β -zeolite, Y-zeolite, HZSM-5 and mordenite) during vapor phase upgrading of pine pyrolysis products. Their results showed that the chemical composition of the resulting oil depended on the structure of the acidic zeolite; however, the yield of oil was only slightly dependent on the structure. In another study, Aho et al.,⁴⁰ investigated the influence of acidity for β -zeolites on the yield and the chemical composition of upgraded bio-oils by changing the silica-to-alumina ratio (SAR 25, 150 and 300). They found that higher acidity (low SAR) β -zeolites produced less organic oil, and more water and polyaromatic hydrocarbons (PAHs). The organic oils produced from upgrading pine pyrolysis vapors using these three β -zeolite catalysts were composed of aldehydes, acids, alcohols, ketones, phenols, and PAHs. These same compounds (with the exception of the PAHs) were also found in the organic oil produced from passing pine vapors over quartz sand. Levoglucosan was also found in the organic oil for β -zeolite with a SAR of 300. In their study the biomass-to-catalyst ratio was high, 2.5, which could be high enough to cause breakthrough of some of the primary pyrolysis products.

The objective of this work is to determine the effect of acid sites on product distribution, yields and coking during vapor phase upgrading of pine pyrolysis products. This was achieved by testing a suite of β -zeolites with widely varying silica-to-alumina ratios (SAR = 21, 25, 38, 75, 250) using real-time measurement of the composition of the upgraded pyrolysis vapors to track product composition and catalyst deactivation. In an earlier study⁴¹ it was demonstrated that the different levels for deactivation of HZSM-5 catalyst, which is related to the biomass-to-catalyst ratio, impacts product distribution during upgrading of biomass pyrolysis vapors. This catalyst completely deoxygenates biomass vapors to form olefins and aromatic hydrocarbons until a biomass-to-catalyst ratio of approximately 0.2 (w/w). At a biomass-to-catalyst ratio of 0.3 a suite of products comprising furans, phenol and cresols were observed. Finally, the primary

vapors started to breakthrough at a biomass-to-catalyst ratio of 0.6. HZSM-5 has a three dimensional pore system consisting of straight 10 member ring $5 \times 5 \text{ \AA}^2$ channels linked by sinusoidal channels.^{39, 42} Due to differences in pore structure and other morphological features, we hypothesized that β -zeolites would give different products with respect to the level of deactivation. In order to investigate the effect of pore structure on product distribution and coking, in this study we investigated the effect of β -zeolites on upgrading of pine pyrolysis vapors. β -zeolites have a three dimensional pore structure comprising a 12 ring channel with $7.5 \times 6.5 \text{ \AA}^2$ pores plus two perpendicular 12 ring channels with $7.5 \times 6.5 \text{ \AA}^2$ and $5 \times 5 \text{ \AA}^2$ pores^{39, 42}. These characteristics represent a different channel structure plus larger pores than HZSM-5.

2. Experimental set-up.

2.1 Materials

Southern yellow pine supplied by Idaho National Laboratory (INL) and ground to fine powder (120 μm) was used as biomass in the experiments. The elemental analysis of this feedstock shows that it contains 52 % carbon, 41 % oxygen, 6 % hydrogen and less than 1 % nitrogen. The water content was 2.9%.

The β -zeolites used in this study were in powder form (sieved to 38-150 μm) and supplied by Johnson Matthey LLC and are commercially available in the ammonium form. The acid form was obtained by calcination in flowing air (3 l/min) before use with heating at 1 $^\circ\text{C}/\text{min}$ to 70 $^\circ\text{C}$ and holding for 4 hours. The catalyst was then heated at 1 $^\circ\text{C}/\text{min}$ to 110 $^\circ\text{C}$ and held at this temperature for 4 hours. Finally the catalyst was heated at 1 $^\circ\text{C}/\text{min}$ to 500 $^\circ\text{C}$ and held for 4 hours before cooling to room temperature.

2.2. Characterization of Catalysts

2.2.1 Nitrogen physisorption. The samples were analyzed on a Micromeritics 2420 physisorption analyzer using nitrogen gas at 77K to measure an adsorption-desorption isotherm comprising approximately 63 adsorption and 40 desorption data points. The adsorption isotherm covered the relative pressure range of 0.003 to 0.995 and the final desorption point was taken at approximately 0.005 P/Po. The samples were pre-treated under vacuum at 350 $^\circ\text{C}$ for 16 hours on the instrument degas stations prior to analysis before transferring to the analysis ports. Non return seal frits were used to stopper the tubes to prevent the ingress of air during re-weighing and transfer. Approximately 63 adsorption and 40 desorption data points were taken. The Rouquerol method was used to determine the best range of linearity for the BET equation to yield the apparent BET surface area.

2.2.2 X-ray Diffraction (XRD). The β -zeolite phases were confirmed using XRD on a Bruker D8 spectrometer. The spectra were recorded with a Cu K α emission wavelength of 1.5406 \AA at 0.02 $2\theta/\text{s}$.

2.2.3 NH₃ temperature-programmed desorption (TPD). In order to quantify the number of acid sites on the catalyst materials, NH₃ TPD was conducted with the assumed stoichiometry of one NH₃ molecule adsorbed per acid site. Catalyst samples (200 mg) were loaded in a quartz U-tube and evaluated on a micro-flow reactor system (AMI-390) equipped with a thermal conductivity detector. Catalysts were pretreated by heating in 10 % O₂/Ar to 500 $^\circ\text{C}$ and held for 60 min, and then cooled to 120 $^\circ\text{C}$ in He flow following which the adsorption step was performed. This consisted of flowing 10 % NH₃/He for 30 min at 120 $^\circ\text{C}$, followed by flushing with He. The TPD was performed by heating at 30 $^\circ\text{C}/\text{min}$ from 120-500 $^\circ\text{C}$, with a 30 min hold at 500 $^\circ\text{C}$. The gas flow rate in all steps was 25 sccm. A sample loop of known volume was used to calibrate the thermal conductivity detector (TCD) response for NH₃, and quantify the amount of NH₃ desorbed from the samples.

2.2.4 Pyridine-IR

Comparative characterization of the Brønsted and Lewis acid sites in the β -zeolites was carried out using transmittance FTIR measurements in the 4000-1200 cm^{-1} spectral range. FTIR transmittance measurements were performed at $\sim 30 \text{ }^\circ\text{C}$ using self-supported disks activated at 450 $^\circ\text{C}$ for 6 hours in vacuum (with a temperature ramp of 1 $^\circ\text{C}/\text{min}$). FTIR spectra were collected using a Nicolet Protege 460 spectrometer at a 2 cm^{-1} resolution (0.96 cm^{-1} data spacing). The spectra were analyzed using the Omnic software from Nicolet. Accuracy of the maximum positions was estimated to be $\pm 1 \text{ cm}^{-1}$ for $\nu_{0 \rightarrow 1}$ lines. Acidic properties of the samples were evaluated using temperature programmed desorption of pyridine monitored spectroscopically. An excess of pyridine was admitted into the transmittance cell at a specified temperature, 150 $^\circ\text{C}$ in this work, in a stepwise manner until no changes were observed in the spectra. The saturated sample was then evacuated for 5 min at 150 $^\circ\text{C}$ to remove physically adsorbed pyridine and the FTIR spectrum collected. The intensity of the Lewis and Brønsted acid peaks at approximately 1455 and 1545 cm^{-1} , respectively, were obtained at 150 $^\circ\text{C}$, and the B/L ratio was used in conjunction with the total acidity obtained via NH₃ TPD to generate the reported Brønsted and Lewis acidities for the catalysts.

2.3 Horizontal Reactor-MBMS

A semi-batch reactor system was used to study deactivation of the suite of β -zeolites; a detailed description of this system has been reported previously.⁴¹ This reactor is a horizontal quartz annular flow tube in which boats of biomass are pyrolyzed and the vapors flow through a fixed catalyst bed. The products are measured with a molecular beam mass spectrometer (py-MBMS).¹⁹ Pyrolysis and vapor upgrading takes place in the inner tube where the vapors were entrained in a 0.4 slm flow of helium. The flow in the inner tube is diluted with a 4 slm helium stream from the outer tube in order to dilute the products and minimize secondary reactions before the vapor stream is sampled by the MBMS orifice. The reactor is heated to the desired temperature using a five-zone furnace.

The catalyst bed was prepared by suspending the catalyst on quartz wool. The integrity of the bed was checked by measuring the pressure drop across the bed both at room temperature (~ 9 torr) and at 500 °C (~ 31 torr). During the experiment, quartz boats containing 50 mg of pine were introduced at a rate of approximately one every 120 seconds into the pyrolysis zone of the inner tube which was maintained at 500°C. Approximately 40 boats were consecutively pyrolyzed during a typical experiment using a fixed bed of 0.5 g β -zeolite catalyst. Each pulse of pyrolysis vapor lasted for about 60 seconds, and assuming a 60 % pyrolysis vapor yield, the weight hourly space velocity is estimated to be about 3.6 h⁻¹. The catalytically upgraded vapors resulting from each periodic addition of biomass were then sampled by the MBMS orifice.

The MBMS^{17-19, 41, 43, 44} has been shown to be effective for direct, real-time analysis of biomass pyrolysis and vapor phase upgrading. The universal detection afforded by mass spectrometry allows measurement of the entire complex suite of molecules produced during pyrolysis and upgrading. Molecular beam sampling enables direct measurements from hot, dirty environments with better than 1 second time resolution. With this time resolution, transient catalyst behavior and deactivation can be directly monitored. The adiabatic cooling in the molecular beam and the low ionization energy (22.5 eV) greatly reduces fragmentation, which simplifies the spectra of the products. The disadvantages of the MBMS are: 1) it collects very complex product spectra that are often best analyzed using multivariate analysis techniques as described below and; 2) it is difficult to distinguish different ions with the same nominal mass. As discussed below, in this study we used complimentary GCMS data to identify some of the products in order to resolve this ambiguity.

In the MBMS the upgraded vapors and gases undergo adiabatic expansion through an orifice (250 μ m) into a vacuum chamber (~ 100 mtorr). This expansion cools the gas and the cooled gas is skimmed into a molecular beam, which is ionized by 22.5 eV electron impact. The positive ions are then measured using a quadrupole mass spectrometer. A mass spectrum with an m/z range of 10-500 is collected every second. A small, precisely controlled flow of argon (40 sccm) mixed with He carrier gas is used as a tracer gas.

2.3.1 Multivariate Analysis of MBMS Spectra. Multivariate analysis was used to identify groups of mass spectral peaks that were correlated in the product vapors and to track their trends as the catalyst deactivated. We used the multivariate curve resolution optimized by alternating least squares (MCR-ALS) routine available in the statistical analysis software package The Unscrambler (Camo Software AS, version 9.7). In our analysis, we included constraints for producing non-negative concentration profiles and non-negative mass spectra. We did not apply constraints for unimodality and equality in concentration profiles so that the variation of relative concentrations for pure components (PCs) with biomass-to-catalyst ratio represents the data accurately. Further details on the application of multivariate analysis on biomass pyrolysis and gasification can be found elsewhere.^{17, 41, 44, 45}

2.4 Tandem micropyrolyzer-GCMS

A tandem micropyrolyzer (Rx-3050TR, Frontier Laboratories, Japan) equipped with an autosampler (AS-1020E) and a microjet cryo-trap (MJT-1030Ex) coupled to a GCMS was used to complement the py-MBMS vapor phase upgrading experiments. The micropyrolyzer consists of two heating zones, one for pyrolysis and another for catalytic vapor phase upgrading of the pyrolysis products. Pine samples loaded in deactivated stainless steel cups were automatically dropped in the pyrolysis zone using the autosampler. A fixed bed of the catalyst was placed in the vapor phase upgrading zone. A liquid nitrogen trap was placed after the upgrading zone to adsorb the product vapors which were subsequently desorbed into the inlet of the GC (7890B, Agilent Technologies, USA) interfaced with the MS (5977A, Agilent Technologies, USA). To monitor deactivation of the β -zeolites, several 0.5 mg samples were pyrolyzed consecutively and the vapors were passed through a fixed bed containing 4 mg catalyst until the total biomass-to-catalyst ratio was ~ 2 (w/w). During the experiment, products from the pyrolysis zone (500 °C) entrained in He carrier gas flowed through the upgrading zone (500 °C) and then through the liquid nitrogen trap (-196 °C). Some non-condensable light gases passed through the trap, but condensable gases and all condensable vapors were adsorbed. The trapped gases and vapors were separated in a capillary column (Ultra Alloy-5, Frontier Laboratories, Japan) with a 5 % diphenyl and 95 % dimethylpolysiloxane stationary phase. The liquid nitrogen trap was housed inside the GC oven, which was programmed as follows: hold at 40 °C for 2 min then ramp to 325 °C at a rate of 10 °C min⁻¹. The separated upgraded species were identified using the NIST GCMS library. Some products were identified by comparing the retention times and mass spectral fragmentation patterns to standards that were injected separately. A smaller set of 9 compounds was used to calibrate the instrument to allow for quantification.

2.5 Coke Analysis

The amount of coke deposited on the catalyst was measured by thermogravimetric analysis in a TGA Instruments Q500 analyzer. The spent catalysts were heated in air at 20 °C/min from 25 °C to 850 °C. The mass loss from 250 to 850 °C was attributed to coke and that below 250 °C was due to water and weakly adsorbed organic species. Extraction of coke from spent catalysts using CH₂Cl₂ was attempted, but did not yield any soluble material.

3. Results and Discussion

3.1 Catalyst characterization

The results for characterization of each of the five β -zeolites (SAR 21, 25, 38, 75 and 250) are shown in Table 1. The pore volumes, pore size distributions and BET surface area were determined from nitrogen physisorption. The crystallite sizes were calculated using the Scherrer equation. These data confirmed that all five zeolites were of the β -zeolite phase

and had similar crystallite sizes. The total acid sites were measured using NH_3 TPD. As expected, the number of total acid sites was found to increase with decreasing SAR. The Brønsted and Lewis acid sites were determined from pyridine IR. Table 1 shows the results from pyridine-IR.

3.2 Py-MBMS

3.2.1. Pine VPU using zeolites. Upgrading of pine pyrolysis vapor over zeolites can lead to significant simplification of the vapor product suite and oxygen rejection. Fig. 1 compares mass spectra obtained from raw pyrolysis vapors and from a single boat of biomass run through the horizontal reactor containing fresh 0.5 g of SAR 25 beta zeolite. The molecular species in the raw pyrolysis vapor mass spectrum in Fig. 1A have been identified in numerous previous publications, and include organic acids, esters, aldehydes, alcohols, furans, sugars and anhydrosugars, phenolics and substituted aromatics.^{17, 28, 46, 47} Nearly all of the molecules in the pyrolysis vapors contain at least one oxygen atom and there are hundreds of individual species. In the mass spectrum of the upgraded vapors shown in Fig. 1B, the number of products is greatly reduced and, as shown below, none of the organic species identified contain oxygen. The organic molecules in this spectrum are primarily small olefins, benzene, alkylated benzenes, naphthalene, alkylated naphthalenes, anthracene and alkylated anthracenes. The identities of these products were confirmed with the GCMS system. The mass-to-charge ratios (m/z) of some of the more intense peaks in the mass spectra have been identified and the number of observed peaks indicates the total number of products. For the spectrum of the raw vapors, 186 mass spectral peaks between m/z 10 and 210 have intensity greater than 1% of the maximum while for the upgraded spectrum there are only 54 peaks above this threshold. This shows how the complexity and number of products are greatly reduced by upgrading as is consistent with observed experimental results.^{7-15, 17-35, 16, 14, 32, 41}

Though vapor phase upgrading using a fresh catalyst can significantly reduce the complexity and the amount of oxygen in the pyrolysis products, the yields of observed oils are typically low. Experimental yields of oil from upgrading using fresh catalyst are normally about 10 – 15%.^{14, 32, 41, 47} This is a result of the buildup of carbon on the catalyst, generally referred to as coke, and losses due to light gas formation. In order to optimize the oil yields and minimize the formation of oxygenated products, it is necessary to understand the deactivation process. Thus, we investigated the mass spectra of vapor phase products during sequential introduction of pyrolysis vapors over a fixed bed of the SAR 25 catalyst.

Fig. 2 shows the variation of selected mass spectral peaks from Fig. 1 with each subsequent sample boat pyrolyzed. The sums of peaks at m/z 78, 92 and 106, likely benzene, toluene and xylenes, represent the upgraded products as shown in Fig. 1B, while the peaks at m/z 126, 137 and 164 (5-hydroxymethylfurfural, 4-methylguaiacol and isoeugenol¹⁷) are peaks from the raw pyrolysis vapor spectrum, Fig. 1A. Each 50 mg boat resulted in a pulse of ion signal for these different species.

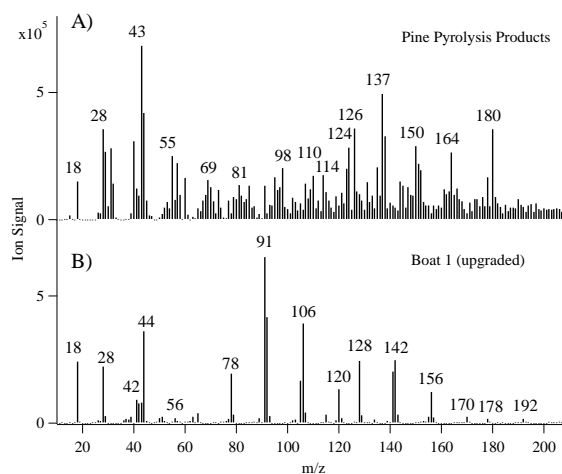


Fig. 1 A) Mass spectrum of raw pine pyrolysis vapors and B) the products from upgrading these vapors over a fresh β -zeolite (SAR 25) using the horizontal reactor-MBMS system at 500°C.

The intensities of the selected upgraded products (Fig. 2B) remain constant with each subsequent boat until boat 5 (biomass-to-catalyst ratio of 0.5), and then start to decrease. The two- and three-ring aromatic products, m/z 128, 142, 156, 170 (naphthalene, methyl-naphthalene, dimethyl and trimethyl naphthalenes) and m/z 178, 192 and 206 (anthracene and methyl- and dimethyl anthracenes) shown in Fig. 1B increase from boat 1 to boat 5, then decrease. This is shown in Fig. S1 in the Supplementary Materials. Note that the species m/z 170, 178, 192 and 206 are negligible in the first pulse as shown in Fig. 1B. These species are more prominent than was seen in studies using HZSM-5,⁴¹ which is likely a result of the larger pore sizes of the β -zeolite compared to HZSM-5 (5.95 Å vs. 4.7 Å)⁴². The multi-ring compounds are also likely precursors to the formation of graphitic coke on the catalyst.

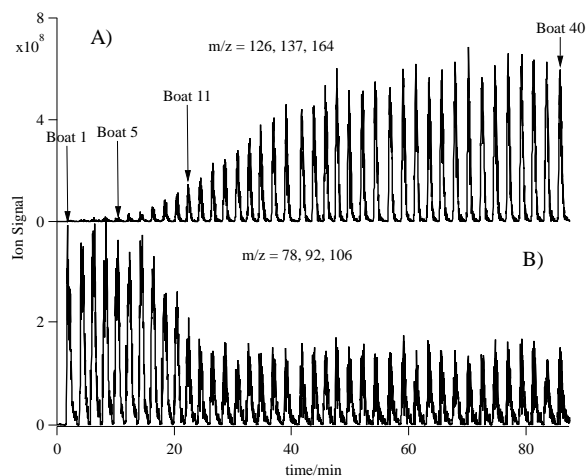


Fig 2. Ion signals for mass spectral peaks from Fig. 1 during the vapor phase upgrading of pyrolysis of 40 boats, each containing 50 mg of pine, and the vapors passed over a fixed

bed containing 0.5 g β -zeolite (SAR 25). The pulses in A) are from the raw pyrolysis spectrum, while the pulses in B) are from the upgraded products.

After boat 5, oxygenated molecules start to breakthrough and the activity decreases. The peaks for the raw pyrolysis products were nearly absent during during boat 1, and then gradually increased until about boat 30, where the signal leveled off indicating that the catalyst is fully deactivated due to the buildup of carbon on the catalyst as more biomass vapors pass through the bed. After about 30 boats, the catalyst is completely deactivated and the products mass spectrum is very similar to that obtained for raw pyrolysis vapors, Fig. 1A. In effect, these experiments illustrate the changes in products during deactivation of the upgrading catalyst.

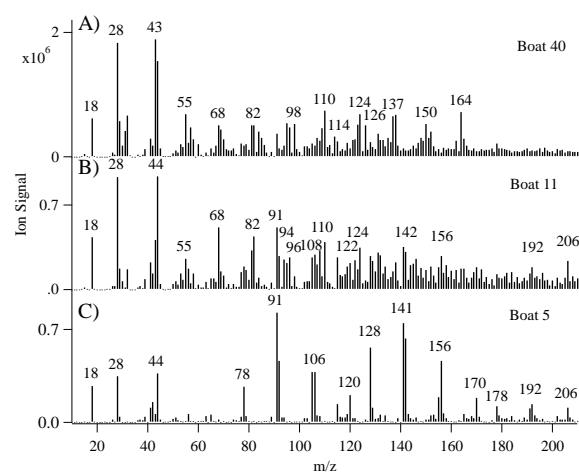


Fig. 3 Averaged mass spectra for pyrolysis and upgrading of pine vapors recorded from boats 5, 11 and 40 (β -zeolite with SAR 25).

Fig. 3 shows additional mass spectra averaged at different points of the experiment, revealing the chemical changes in the products as the catalyst ages. The vapor composition for boat 1 in Fig. 1B and boat 5 in Fig. 3 consist of mostly deoxygenated hydrocarbons (olefins and aromatics). Inspection of the peaks seen in Fig. 1B (boat 1) and 3C (boat 5) show that as the catalyst ages, more 2- and 3-ring aromatic species are present in the product vapors. For instance methyl naphthalenes, (m/z 142), dimethyl naphthalenes (m/z 156), anthracene and alkyl anthracenes (m/z 178, 192, 206) are all more intense in Fig. 3C than Fig. 1B. The increased presence of these compounds in the products could be due to a change in catalyst selectivity by deactivation, or simply expulsion of these compounds from the catalyst due to a buildup of material in the catalyst pores such that larger molecules can no longer be accommodated. Other researchers have suggested that β -zeolites are the best catalysts for upgrading biomass to form small aromatics, such as benzene and toluene.³⁶ The data in Figs. 1 and 3 (above) show that this is true when the biomass-to-catalyst ratio is low. The mass spectrum that results from boat 40 (biomass-to-catalyst ratio of 4) consists of peaks that are similar to those in the pine primary vapors, suggesting complete deactivation. As can be seen in Fig. 3A, many of the prominent peaks in this

spectrum are also seen in Fig. 1A for the raw pyrolysis vapors. There are a few notable exceptions such as m/z 180, which is likely coniferyl alcohol and m/z 60, which is acetic acid or hydroxyacetaldehyde. These compounds could react with the carbonized, deactivated catalyst and be removed from the product stream.

The spectrum collected during the introduction of boat 11 shows that the products observed during partial deactivation are not a simple combination of the products measured when the catalyst is fully active and when it is deactivated. The spectrum for boat 11 (biomass-to-catalyst ratio of 1.1) consists of products with peaks found in spectra for both boats 1 and 40, plus additional new peaks. Note the prominence of the peaks in Fig. 3B at m/z 94, 108 and 122 (phenol, methyl phenols and dimethyl phenols) and at m/z 68, 82 and 96 (furan, methyl furans and dimethyl furans). The trends of these species along with aromatics, and the raw pyrolysis products are shown in Fig. S2, in Supplementary Materials. The mass spectral peaks for the phenols and furans grow faster with added biomass than the peaks for the raw pyrolysis products. We hypothesize that these species are intermediates in the deoxygenation process and that they desorb without further deoxygenation as the micropores of the catalyst start to become filled with coke and coke precursors.

In order to more accurately identify product trends occurring during catalyst deactivation, we employed multivariate analysis (MCR-ALS) for a dataset containing all of the mass spectra over an 80 min window for each of the 40 pulses shown in Fig. 2. MCR-ALS has been applied to mathematically decompose data with overlapping mass spectra during vapor phase upgrading of biomass pyrolysis products using HZSM-5,⁴¹ and the theory of MCR-ALS analysis can be found elsewhere.^{17, 45} The MCR-ALS analysis produces two outputs: 1) a loadings plot, which groups products (mass spectral peaks) that are correlated, and; 2) a scores plot, which shows how the grouped mass spectra (loadings plot) changes during the course of the experiment. The top 130 out of 500 masses with the largest variances were selected for this analysis, resulting in a data set with dimensions of 40 boats x 130 masses. The MCR-ALS analysis was optimized to produce three pure components (PCs). Increasing the PCs beyond three did not cause a significant change in the residual error. Fig. 4 shows the loadings plots for these three PCs. As can be seen, PC 1 contains deoxygenated hydrocarbons similar to the mass spectrum recorded for boat 5. This is the mass spectrum obtained when pine pyrolysis vapors were passed over fully active catalyst.

PC 3 contains pine primary vapors similar to the spectrum for boat 40. This is the mass spectrum obtained when pine primary vapors were passed over a deactivated catalyst. PC 2 contains mass spectral peaks for furan, phenol, methylated furans and phenols discussed above as well as benzofuran m/z 132, catechol m/z 110, methoxyphenol m/z 124 and methyl methoxyphenol m/z 138. Phenols and furans arise from reactive intermediates formed during upgrading of pine vapors with the catalyst.⁴¹ Thus, PC 1 contains products formed from a fully active β -zeolite, PC 2 contains

oxygenated intermediates and PC 3 contains oxygenated pine primary pyrolysis vapor.

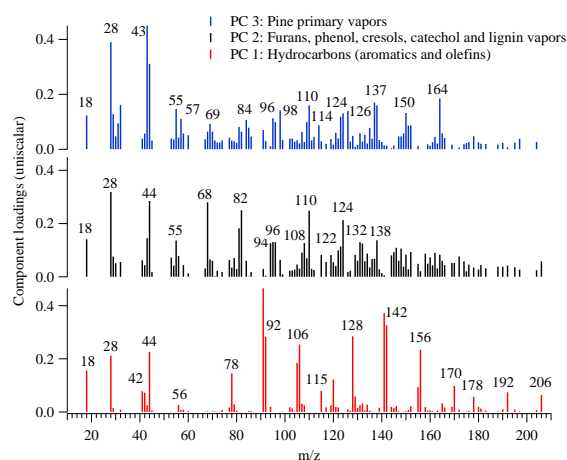


Fig. 4 Reconstructed spectra for each pure component (PC 1 to PC 3) from MCR-ALS analysis of upgrading pine vapors over β -zeolite (SAR 25) revealing changes in the composition of the product stream as the catalyst deactivates. Note: the reconstructed spectra are unit-vector normalized.

The plots for the scores of these three PCs as a function of biomass-to-catalyst ratio are shown in Fig. 5. Initially, only olefins and aromatic molecules (PC 1) are observed because the catalyst is still fully active and able to completely deoxygenate pine pyrolysis vapors. The signal for this component increases until a biomass-to-catalyst ratio of 0.5. This increase is due to increases in naphthalenes and anthracenes as discussed above and shown in Fig. S1 in Supplementary Materials.

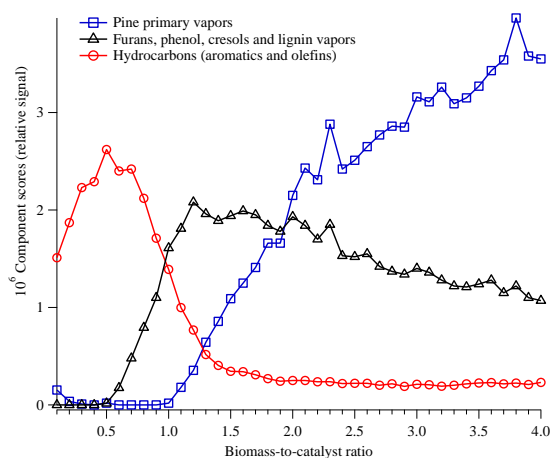


Fig. 5 The component scores from MCR-ALS analysis of vapor phase upgrading experiment showing the dependency of each PC with biomass-to-catalyst ratio for β -zeolite with SAR 25. The loadings spectra are shown in Fig. 3.

After a biomass-to-catalyst ratio of about 0.5 (Fig. 5), PC 1 decreases sharply until a biomass-to-catalyst ratio of 1.5, and stays constant throughout the remainder of the experiment

indicating that the catalyst's selectivity for production of hydrocarbons has declined to nearly zero. The concentration of oxygenated intermediates in the product vapors (PC 2) begins to increase starting at a biomass-to-catalyst ratio of 0.6, reaches a maximum at approximately 1.2, and then decreases slowly throughout the remainder of the experiment. This could be due to a build-up of methylated aromatics in the catalyst pores. Previous methanol-to-olefin (MTO) studies have shown that increasing the methyl-substituted aromatics inside zeolite pores greatly influenced the selectivity and activity of the catalysts.^{48, 49} The observation of phenol and cresols in PC 2 could be due to these compounds being held tightly inside the catalyst pores because they are polar as opposed to the non-polar aromatic hydrocarbons. In addition, coke precursors such as methylated multi-ring aromatics will continue to grow inside the pores, which can prevent some biomass vapors from getting into the catalyst pores and hence unreacted vapors will pass through the bed as is seen in Fig. 5 starting at a biomass-to-catalyst ratio of 1.1 (PC 3). PC 3 grows continuously throughout the experiment until the catalyst is completely deactivated. PC 3 starts to dominate at a ratio of 2.0 indicating that the majority of the catalyst is deactivated.^{25, 41}

3.3 Py-GCMS

3.3.1 Product identification. The MBMS provides a real-time snapshot of the products formed during vapor phase upgrading. Py-GCMS compliments this technique by allowing identification of structural isomers. Fig. 6 compares MBMS and GCMS results for upgrading over fresh catalyst. The chromatogram in the lower panel of Fig. 6 was recorded from the first pulse of pyrolysis vapors and the mass spectrum in the upper panel was recorded from boat 1 (biomass-to-catalysts ratio of 0.125). Both figures show that a fresh β -zeolite completely deoxygenates pyrolysis products to form mostly aromatic hydrocarbons. Fig. 6 shows that the MBMS is very good at separating light gases (H_2O m/z 18, CO m/z 28, CO_2 m/z 44, and $\text{C}_2\text{-C}_4$ olefins m/z 28, 42 and 56).

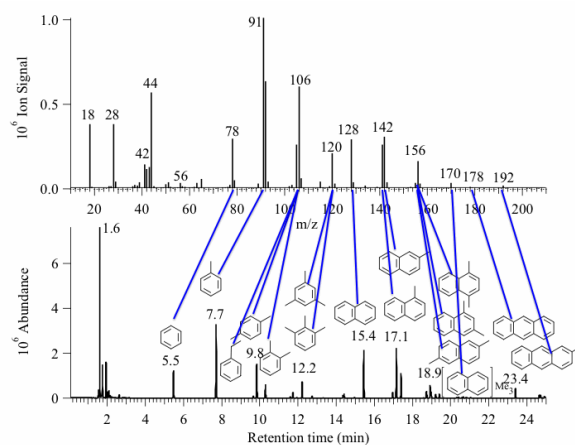


Fig. 6 Comparison of MBMS and GCMS results from upgrading pine pyrolysis products using fresh β -zeolites (SAR 25). Pyrolysis and upgrading temperatures were set at

500 °C. Correlations between products identified using GCMS and m/z peaks in MBMS are shown with blue lines.

The MBMS is also a high throughput technique as shown in Fig. 2 (40 samples in 90 minutes) as compared to two samples in 90 minutes for the GCMS. In the chromatograph at the bottom, the GCMS readily distinguishes structural isomers, for example; species labelled m/z 106 on the MBMS are clearly speciated into ethyl benzene, *p*-xylene and *o*-xylene by GCMS. However, the py-GCMS system used for this work, with a liquid nitrogen trap, is not ideal for separating light gases, especially those with boiling points below -196 °C.

The mass spectrum and chromatogram both contain intense peaks for one- and two-ring aromatics, as discussed above. Smaller peaks are observed for the 3-ring aromatic compounds. Complete results from the py-GCMS study using the SAR 25 catalyst are shown in Table 2, which lists the structures and compounds identified for chromatograms recorded when the cumulative biomass-to-catalyst ratios were 0.125, 1.1 and 2. An interesting trend observed from the GCMS data is that molecules with smaller kinetic diameters appear to be present in larger amounts. For instance, the peak for *p*-xylene is almost twice that of *o*-xylene and *m*-xylene is not observed. Likewise, the peak for 2-methylnaphthalene is twice as large as 1-methylnaphthalene and anthracene is observed while phenanthrene is not. This is likely due to greater mobility of the more compact molecules relative to their less compact and more bulky structural isomers.

GCMS has also been used to confirm the structures of some of the oxygenated compounds that appear during partial deactivation. The chromatogram recorded at a biomass-to-catalyst ratio of 1.1 contains hydrocarbons plus some oxygenated species, which agrees well with the results from py-MBMS (Fig. 5). The oxygenated species observed at this ratio include furan, 2-methyl furan, 3-methyl furan, 2,5-dimethyl furan, benzofuran, and 2-methyl benzofuran; this is in good agreement with species identified in PC 2 of Fig. 4. Phenol, 2-methyl phenol and 3-methyl phenol (cresols) are also observed. Acetaldehyde m/z 44 and acetone m/z 58 are the only primary vapor molecules observed at this ratio. These molecules could be part of PC 2 above since their m/z overlaps with species observed in this PC. The hydrocarbons observed at this ratio include olefins (propene and 2-butene) and aromatics (benzene, toluene, ethyl benzene, *p*-xylene, *o*-xylene, 1-ethyl-3-methyl benzene, 1,3,5 trimethyl benzene, indene, indane, naphthalene, 2-methyl naphthalene and 1,3 dimethyl naphthalene).

Highly methylated naphthalenes, trimethyl and tetramethyl, which were very weak at a biomass-to-catalyst ratio of 0.125 are also observed at the biomass-to-catalyst ratio of 1.1, in agreement with the results for the horizontal reactor (boat 1 and boat 5 in the discussion above). The chromatogram recorded at a ratio of 2 contains mainly primary vapors and furans, phenol and cresols and a few aromatic compounds.

3.3.2 Product trends. The GCMS data also confirms the trends in product formation measured with the MBMS. Standards were prepared to identify and quantify some

compounds observed during the vapor phase upgrading experiment. Fig. 7 shows the variation of yields for representative compounds of the three groups of products observed in Figs. 4 and 5, that is, aromatic hydrocarbons, furans and phenols, and primary vapors. The results in Fig. 7 show similar trends to the py-MBMS Figs; hydrocarbons are formed at low biomass-to-catalyst ratios, the furans and phenols breakthrough at about 0.5 compared to 0.5 in Fig. 5 and the primary vapors (guaiacol) breakthrough at 1.3 compared to 1.0 in Fig. 5.

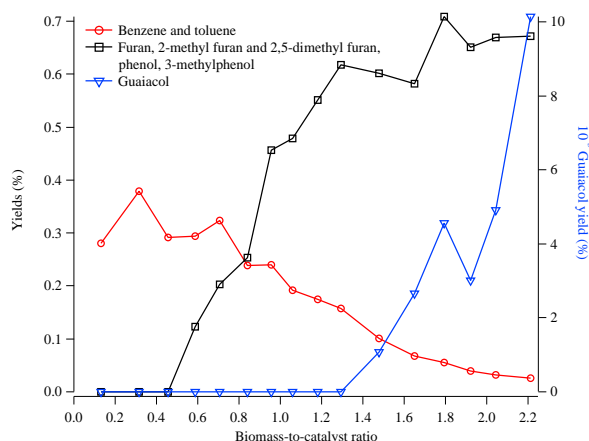


Fig. 7 The effect of biomass-to-catalyst ratio on vapor phase upgrading of pine pyrolysis products. Pyrolysis and vapor phase upgrading experiments were done using the tandem py-GCMS system with temperatures set at 500 °C. Right axis: guaiacol yield. Left axis: yields for aromatics, furans, phenol and cresols.

Figs. 5 and 7 can be used to tune the products from the upgrading experiment. For example, a bio-oil with low oxygen content can be prepared if the biomass-to-catalyst ratio is less than 0.5. However, this results in low oil yields. A higher oil yield can be obtained if the ratio is between 0.8 and 1.2. This is, however, accompanied by higher oxygen content because in addition to aromatics, the oil will also contain furans, phenol and cresols (Figs. 5 and 7). Oil collected at a biomass-to-catalyst ratio greater than 1.2 will contain organic oxygenates that are characteristic of primary vapors. We believe that the product distributions observed in these micro-scale systems should be similar to the composition of oil obtained from large-scale VPU of pine using β -zeolites. This is because we demonstrated that results obtained from these microreactors were in very good agreement with results from a bench-scale fluid bed reactor.¹⁴

3.4 Effects of number of acid sites

Similar py-MBMS experiments conducted with the other four β -zeolites, SAR 21, 38, 75 and 250 showed as expected that deactivation occurred at a smaller biomass-to-catalyst ratio with decreasing number of acid sites. As with the SAR 25 catalyst, 40 boats containing 50 mg of pine were pyrolyzed sequentially and the vapors were fed through the catalyst beds for the other β -zeolites. For each experiment we used MCR-ALS to analyze the resulting 40 x 130 data sets and

extracted three pure components. As an example, Fig. 8 shows the resulting loadings spectra obtained for the SAR 250 β -zeolite. Because of the small number of acid sites in this catalyst, PC 1 consists of a mixture of deoxygenated and oxygenated products. The oxygenated products observed include furan m/z 68, methyl furan m/z 82, methyl benzofuran m/z 132, dimethyl benzofurans m/z 146, phenol m/z 94, cresols m/z 108, methyl cresols m/z 122 and naphthalenol m/z 144. The deoxygenated products in this PC are propylene m/z 42, butenes m/z 56, butane m/z 58, benzene m/z 78, toluene m/z 92, xylenes or ethyl benzene m/z 106, trimethyl benzenes or ethyl toluenes m/z 120, naphthalene m/z 128, methyl naphthalenes m/z 142, dimethyl naphthalenes m/z 156, trimethyl naphthalenes m/z 170 and tetramethyl naphthalenes m/z 184 (Table 2). This is different from the data of the SAR 25 β -zeolite where PC 1 consisted of only olefins and aromatic hydrocarbons (including anthracenes m/z 178, 192 and 206).

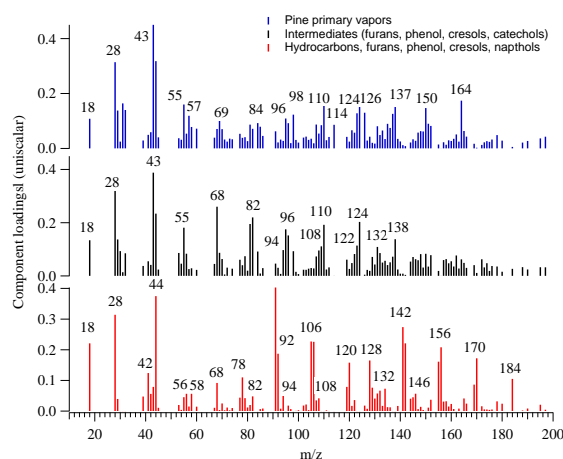


Fig. 8 The reconstructed spectra for each pure component (PC 1 to PC 3) from MCR-ALS analysis of upgrading pine vapors over β -zeolite (SAR 250) revealing changes in the composition of the product stream as the catalyst deactivates. Note that the reconstructed spectra are unit-vector normalized.

Further evidence of these differences can be found in the spectrum recorded from upgrading pine vapors from the first boat (Fig. S3 in Supplementary Materials), which show peaks for furan m/z 68, phenol m/z 94, olefins and aromatic hydrocarbons. This indicates that 0.5 g of the β -zeolite with SAR 250 does not have a sufficient number of acid sites to completely deoxygenate pyrolysis vapors produced from 50 mg of pine (1.24 mmol/g acid sites for SAR 25 compared to only 0.20 mmol/g acid sites for SAR 250). PC 2 and PC 3 for SAR 250 contain the same compounds as PC 2 and PC 3 for SAR 25 (Fig. 4). This is also true for PC 2 and PC 3 of the SAR 21, 38 and 75 β -zeolites (see Figs. S4, S5 and S6 in Supplementary Material).

A plot of the pure component scores as a function of biomass-to-catalyst ratio for the SAR 250 β -zeolite is presented in Fig. 9, which shows more rapid deactivation of this catalyst relative to the SAR 25 catalyst. The figure shows

that PC 1 is observed initially and decreases rapidly until a biomass-to-catalyst ratio of 0.5. PC 2 appears immediately - increases rapidly to a maximum at a ratio of 0.6 - and then decreases gradually throughout the remainder of the experiment. As stated above the selectivity of the catalyst is influenced by the presence of highly methylated aromatics, which are already observed in the spectra for boat 1 (Fig. S1). This results in immediate appearance of PC 2. PC 3 starts to breakthrough at a biomass-to-catalyst ratio of 0.5 and continues to grow throughout the experiment. Even though both PC 2 and PC 3 for the SAR 25 catalyst have the same composition as that of SAR 25 catalyst, they start to appear at lower biomass-to-catalyst ratios than for the SAR 25 catalyst. PC 3 starts to dominate at a biomass-to-catalyst ratio of 1.2 compared to 2.0 for the SAR 25 β -zeolite. The results from the multivariate analysis of deactivation experiments with SAR 21, 38 and 75 are shown in Figs. S4 – S6. It is clearly seen from these plots that deactivation occurs more quickly for zeolites with larger SAR (lower numbers of acid sites).

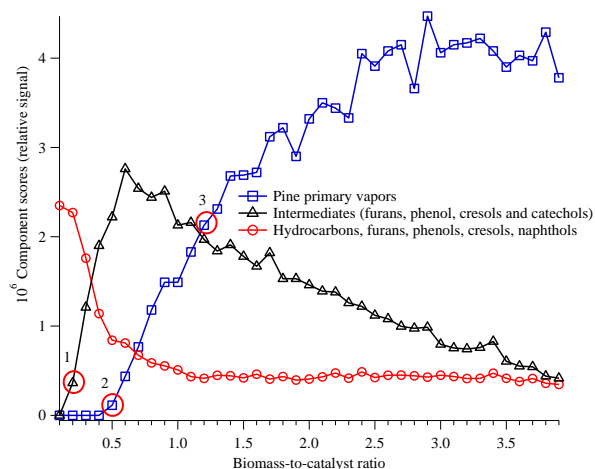


Fig. 9 The component scores from MCR-ALS analysis of vapor phase upgrading experiment show the dependency of each PC with pine-to-catalyst ratio over β -zeolite (SAR 250). The loadings spectra are shown in Fig. 8.

Quantitative comparisons of coke and hydrocarbon yields were made for the catalysts studied during the deactivation process shown in Figs. 5, 9 and S4 – S6. Data taken from three points on these deactivation plots; 1) when intermediates (PC 2) begin to appear; 2) when the primary vapors (PC 3) begin breaking through, and; 3) when the primary vapors dominate (complete deactivation) as indicated by circles on Fig. 9 were used as the basis for these comparisons. Table 1 lists the biomass-to-catalyst ratios of these three points for each catalyst. The data shows that there is a roughly linear increase in the amount of biomass fed until deactivation with respect to total acid sites, which levels off, presumably because of interaction of neighboring acid sites for the SAR 21 and SAR 25 catalysts.

Coke yields were also measured using TGA for each catalyst when the primary vapors began breaking through and at the end of the experiment (a biomass-to-catalyst ratio of 4). During the TGA experiments spent catalysts were heated

from 25 °C to 850 °C in air. The mass loss from 250 to 850 °C was attributed to coke and that below 250 °C was due to water and weakly adsorbed organic species. As can be seen the yield of coke increased with decreasing SAR or increasing number of acid sites. However, since deactivation is dependent upon the number of active sites, the deactivated catalysts were exposed to different amounts of pyrolysis vapors. It is more relevant to consider the amount of coke at a given level of deactivation. Thus, coke measurements were also made when the catalyst started to show breakthrough of primary pyrolysis vapors. Experiments were conducted in which the products were monitored as boats of biomass were added to the horizontal reactor. When primary vapors started to appear, the experiment was stopped and the catalyst was cooled in flowing helium. Coke on the catalyst was measured using TGA and the values are shown in Table 1.

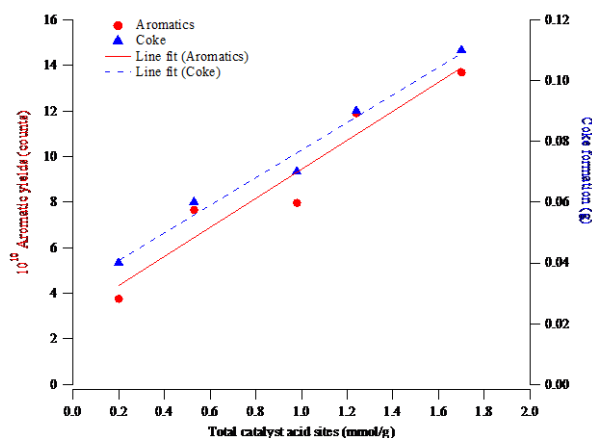


Fig. 10 Total aromatic production and amount of coke deposited on catalysts at the point of primary vapor breakthrough on β -zeolites of varying SAR.

Fig. 10 shows the amount of coke that has been deposited on the catalysts of varying SAR at the point where primary vapors were observed, as well as the total amount of aromatic species that were produced prior to the breakthrough of primary vapors. The coke and aromatic production are plotted as a function of the total acid sites, as determined by NH_3 TPD, with the highest SAR catalyst corresponding to the lowest total acid sites. As expected, an increase in total acid sites led to an increase in the amount of coke that was deposited. Similarly, the increase in the number of acid sites results in a higher yield of aromatics being produced prior to the breakthrough of primary vapors. The linear fit of the increase in coke deposition and aromatics formation with increasing number of acid sites suggests that the chemistry involved in these reactions is relatively unaltered by the local concentration of acid sites, and is more dependent upon the total quantity of acid sites. The extrapolation to zero-acidity for the coke and aromatics yields does not go through the origin of the plot, which indicates that some coke and aromatics production could occur in the absence of acid sites, by passing pine pyrolysis vapors over a hot, microporous non-catalytic material.^{50, 51} Additionally, it is interesting to note that the ratio of coke-deposition to aromatics production

remains essentially constant over the range of acid sites concentrations testing on the catalyst of varying SAR.

Table 1 shows that all five catalysts produced similar coke yields (g coke/g biomass) of approximately 20 wt % of biomass fed. This is consistent with the observation of a constant ratio of coke and aromatic formation (Fig. 10). This means that changing the number of acid sites on β -zeolites does not affect the fraction of biomass that is converted to coke as long as the catalyst is active and no primary vapors are breaking through. This coke yield is higher than what was measured for HZSM-5 collected under the same conditions.^{10, 14, 32, 41}

We also estimated the yields of selected hydrocarbon products, benzene, toluene, ethyl benzene and xylenes. These measurements were made by integrating the ion signals for the MBMS peaks for these species ($m/z = 78, 92, 106$) up to the point when the primary vapors started to appear. Table 1 and Fig. 10 show that the integrated signal of these hydrocarbons increased with number of acid sites. The relative yields of hydrocarbons can be determined by dividing these values by the amount of biomass fed and as shown in Table 1, this yield is roughly constant for all catalysts.

Another interesting comparison can be made by determining the coke yield and hydrocarbon yield at breakthrough as a function of the number of acid sites of the catalyst; these values are shown in Table 1. Both coke yield and hydrocarbon yield increase with increasing SAR or decreasing number of acid sites. It appears that greater separation of the acid sites makes them more efficient at converting the pyrolysis vapors. This could be because on the more acidic zeolites with lower SARs, acid sites have an average physical spacing that is closer than for the higher SAR zeolites. The closer spacing of acid sites increases the likelihood that a reactant molecule interacting with an acid site could block a nearby acid site, rendering it inaccessible to other molecules during the experiment. For the less acidic, higher SAR zeolites, the blocking of active sites by a reactant is less likely because the acid sites are separated by a larger average distance. This could translate to the observed increase in the aromatic production rate per acid site as the SAR is increased. Additionally, there is evidence in the literature that in addition to acidity, catalyst pore structure is important for aromatic production, which was demonstrated on non-acidic materials (e.g. dealuminated zeolites, SBA-15).^{50, 51} This contribution to aromatic production that results from the β -zeolites structure, which is identical amongst the β -zeolites of varying SAR, could also contribute to a higher observed aromatic production rate per acid site on the higher SAR materials. Finally, a ratio of the yield of hydrocarbons to the yield of coke can provide an indication of the ability of the catalyst to direct products towards hydrocarbons instead of coke. As can be seen in Table 1, this ratio of yields is approximately constant for all catalysts. Thus, the number of acid sites did not impact the hydrocarbon/coke branching.

3.5 Comparison with HZSM-5

The results above show that a fresh β -zeolite with enough acid sites will upgrade pine pyrolysis vapors to form olefins and aromatic hydrocarbons. The composition of the upgraded products changes from hydrocarbons to intermediates (e.g. furans, phenols, etc.) and then primary vapors as more pyrolysis vapors are passed through the catalyst bed. A similar product trend was also observed from HZSM-5 with SAR 30. Fig. S7 shows results from the multivariate analysis of similar deactivation experiments using HZSM-5. Olefins and aromatics are formed initially, intermediates are then observed starting at a biomass-to-catalyst ratio of 0.4, and the primary vapors start to breakthrough at a ratio of 1.1. The primary vapors start to breakthrough at the same biomass-to-catalyst ratio as the SAR 25 β -zeolite, however HZSM-5 appears to form more hydrocarbons from the intensities of the scores plots. To test this we also estimated the yields of selected hydrocarbon products, benzene, toluene, ethyl benzene and xylenes from the HZSM-5 study. These measurements were made before breakthrough of primary vapors and the results reveal that HZSM-5 produces four times more hydrocarbons compared to SAR 25 β -zeolite. This agrees with what has been reported in literature.³⁶ Coked HZSM-5 was also collected before primary vapors were observed and the measured coke yield (g coke/g biomass) was 10 wt % compared to 20 wt % for the β -zeolites. It is clear from these results that HZSM-5 performs better than β -zeolites in terms of hydrocarbon and coke yields. We are not sure at the moment how the acidity and structure of each catalyst influence the results. HZSM-5 has ~ 5 Å three dimensional pores with 10 silicon atom rings.⁴² The three dimensional pores are straight in one direction and sinusoidal in the other. On other hand β -zeolite has larger three dimensional straight pores (~ 6 Å) with 12 silicon atom rings.⁴²

4. Conclusions

The following summarizes important results from this study:

1. A fully active β -zeolite effectively upgrades oxygenated pine vapor phase pyrolysis products to form olefins and aromatic hydrocarbons. Fresh β -zeolites initially form one- and two- ring aromatics. When more pyrolysis vapors are introduced, other highly methylated two- ring and alkylated three ring hydrocarbons begin to appear in the spectrum. The intensity of these species increases as the catalyst ages and then decreases to zero as more biomass pyrolysis vapors are processed through the catalyst bed.
2. Between stages of fully active and deactivated catalyst, a suite of oxygenated products comprising furans, benzofurans, phenol, cresols and naphthalenols is observed. This suite of products was observed for all five β -zeolites used in this study. These species were formed immediately in catalysts with few acid sites (SAR 75 and 250).

3. β -zeolites with more acid sites (low SAR) deactivated at a slower rate and retained their activity for formation of hydrocarbons at high biomass-to-catalyst ratios.
4. However, the cumulative coke yields and hydrocarbon yields measured until primary vapor break-through are approximately the same for all five catalysts. The yields of aromatics per measured acid site increase as the silica-to-alumina ratio decreases indicating that a greater separation of the acid sites makes them more efficient at converting the pyrolysis vapors. Further, all catalyst had a similar hydrocarbon/coke branching ratio.

Acknowledgements

This work was supported by the U.S. Department of Energy's Bioenergy Technologies Office (DOE-BETO) Contract No. DE-AC36-08GO28308 with the National Renewable Energy Laboratory and Johnson Matthey. The authors would like to thank Jesse Hensley (NREL) and Vladimir Zholobenko for stimulating discussions.

References

1. A. V. Bridgwater, *Fast Pyrolysis of Biomass: A Handbook*, CPL Press, Newbury, UK, 1999.
2. A. V. Bridgwater, *Fast Pyrolysis of Biomass: A Handbook Volume 2*, CPL Press, Newbury, UK, 2002.
3. A. V. Bridgwater, *Fast Pyrolysis of Biomass: A Handbook Volume 3*, CPL Press, Newbury, UK, 2005.
4. A. Oasmaa, E. Leppamaki, P. Koponen, J. Levander and E. Tapola, in *ACS Symposium Series, Pyrolysis oils from Biomass*, VTT Publications, 1997, vol. 306, pp. 1-87.
5. A. Oasmaa and C. Peacocke, in *VTT Publications* 2001, vol. 450, pp. 1-102.
6. A. Oasmaa and C. Peacocke, in *VTT Publications* 2010, vol. 731, pp. 1-134.
7. J. D. Adjaye and N. N. Bakhshi, *Fuel Processing Technology*, 1995, **45**, 161-183.
8. J. D. Adjaye and N. N. Bakhshi, *Fuel Processing Technology*, 1995, **45**, 185-202.
9. F. A. Agblevor, S. Beis, O. Mante and N. Abdoulmoumine, *Industrial and Engineering Chemistry Research*, 2010, **49**, 3533-3538.
10. F. A. Agblevor, O. Mante, N. Abdoulmoumine and R. McClung, *Energy and Fuels*, 2010, **24**, 4087-4089.
11. E. Antonakou, A. Lappas, M. H. Nilsen, A. Bouzga and M. Stocker, *Fuel*, 2006, **85**, 2202-2212.
12. A. A. Boateng, C. A. Mullen, C. M. McMahan, M. C. Whalen and K. Cornish, *Journal of Analytical and Applied Pyrolysis*, 2010, **87**, 14-23.
13. T. R. Carlson, T. R. Vispute and G. W. Huber, *Chemsuschem*, 2008, **1**, 397-400.
14. S. Czernik, R. French, A. Stanton and K. Lisa, NREL Milestone Report, 2012, p. 12.
15. J. Diebold and J. Scahill, *ACS Symposium Series*, 1988, **376**, 31-40.
16. J. Diebold and J. Scahill, *ACS Symposium Series*, 1988, **376**, 264-276.
17. R. J. Evans and T. A. Milne, *Energy and Fuels*, 1987, **1**, 123-137.
18. R. J. Evans and T. A. Milne, in *Pyrolysis Oils from Biomass*, eds. E. J. Soltes and T. A. Milne, ACS Symposium Series, Washington, DC, 1988, ch. 26, pp. 311-327.
19. R. French and S. Czernik, *Fuel Processing Technology*, 2010, **91**, 25-32.
20. A. G. Gayubo, A. T. Aguayo, A. Atutxa, B. Valle and J. Bilbao, *Journal of Chemical Technology and Biotechnology*, 2005, **80**, 1244-1251.
21. A. G. Gayubo, B. Valle, A. T. Aguayo, M. Olazar and J. Bilbao, *Industrial and Engineering Chemistry Research*, 2010, **49**, 123-131.
22. T. Q. Hoang, X. Zhu, T. Danuthai, L. L. Lobban, D. E. Resasco and R. G. Mallinson, *Energy and Fuels*, 2010, **24**, 3804-3809.
23. P. A. Horne and P. T. Williams, *Journal of Analytical and Applied Pyrolysis*, 1995, **34**, 65-85.
24. C. A. Mullen, A. A. Boateng, D. J. Mihalcik and N. M. Goldberg, *Energy and Fuels*, 2011, **25**, 5444-5451.
25. E. Putun, B. B. Uzun and A. E. Putun, *Energy and Fuels*, 2009, **23**, 2248-2258.
26. S. D. Stefanidis, K. G. Kalogiannis, E. F. Iliopoulou, A. A. Lappas and P. A. Pilavachi, *Bioresource Technology*, 2011, **102**, 8261-8267.
27. M. J. A. Tijmensen, A. P. C. Faaij, C. N. Hamelinck and M. R. M. van Hardeveld, *Biomass and Bioenergy*, 2002, **23**, 129-152.
28. B. Valle, A. G. Gayubo, A. T. Aguayo, M. Olazar and J. Bilbao, *Energy and Fuels*, 2010, **24**, 2060-2070.
29. T. P. Vispute, H. Zhang, A. Sanna, R. Xiao and G. W. Huber, *Science*, 2010, **330**, 1222-1227.
30. S. Vitolo, B. Bresci, M. Seggiani and M. G. Gallo, *Fuel*, 2001, **80**, 17-26.
31. S. Vitolo, M. Seggiani, P. Frediani, G. Ambrosini and L. Politi, *Fuel*, 1999, **78**, 1147-1159.

32. P. T. Williams and N. Nugranad, *Energy*, 2000, **25**, 493-513.
33. A. H. Zacher, D. Santosa, D. C. Elliott and C. D. B. Brown, *TCBiomass 2011*, 2011.
34. H. Zhang, R. Xiao, H. Huang and G. Xiao, *Bioresource Technology*, 2009, **100**, 1428-1434.
35. D. C. Elliott, *Energy and Fuels*, 2007, **21**, 1792-1815.
36. T. R. Carlson, G. A. Tompsett, W. C. Conner and G. W. Huber, *Top. Catal.*, 2009, **52**, 241-252.
37. H. X. Ben and A. J. Ragauskas, *ACS Sustain. Chem. Eng.*, 2013, **1**, 316-324.
38. H. X. Ben and A. J. Ragauskas, *RSC Adv.*, 2012, **2**, 12892-12898.
39. A. Aho, N. Kumar, K. Eranen, T. Salmi, M. Hupa and D. Y. Murzin, *Fuel*, 2008, **87**, 2493-2501.
40. A. Aho, N. Kumar, K. Eränen, T. Salmi, M. Hupa and D. Y. Murzin, *Process Safety and Environmental Protection*, 2007, **85**, 473-480.
41. C. Mukarakate, X. Zhang, A. R. Stanton, D. J. Robichaud, P. N. Ciesielski, K. Malhotra, B. S. Donohoe, E. Gjersing, R. J. Evans, D. S. Heroux, R. Richards, K. Lisa and M. R. Nimlos, *Green Chemistry*, 2014, **16**, 1444-1461.
42. <http://www.iza-structure.org/databases/>.
43. R. J. Evans and T. A. Milne, *Energy and Fuels*, 1987, **1**, 311-319.
44. M. W. Jarvis, T. J. Haas, B. S. Donohoe, J. W. Daily, K. R. Gaston, W. J. Frederick and M. R. Nimlos, *Energy and Fuels*, 2011, **25**, 324-336.
45. E. D. Malinowski, *Factor Analysis in Chemistry*, Wiley, New York, 1991.
46. C. Branca, P. Giudicianni and C. Di Blasi, *Industrial and Engineering Chemistry Research*, 2003, **42**, 3190-3202.
47. M. S. Talmadge, R. M. Baldwin, M. J. Bidy, R. L. McCormick, G. T. Beckham, G. A. Ferguson, S. Czernik, K. A. Magrini-Bair, T. D. Foust, P. D. Metelski, C. Hetrick and M. R. Nimlos, *Green Chemistry*, 2014, **16**, 407-453.
48. D. Mores, J. Kornatowski, U. Olsbye and B. M. Weckhuysen, *Chemistry – A European Journal*, 2011, **17**, 2874-2884.
49. D. Mores, E. Stavitski, M. H. F. Kox, J. Kornatowski, U. Olsbye and B. M. Weckhuysen, *Chemistry – A European Journal*, 2008, **14**, 11320-11327.
50. D. L. Compton, M. A. Jackson, D. J. Mihalcik, C. A. Mullen and A. A. Boateng, *Journal of Analytical and Applied Pyrolysis*, 2011, **90**, 174-181.
51. Y. Zhao, L. Deng, B. Liao, Y. Fu and Q.-X. Guo, *Energy & Fuels*, 2010, **24**, 5735-5740.

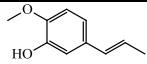
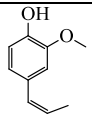
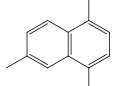
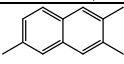
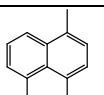
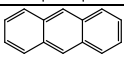
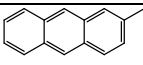
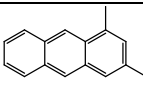
Table 1. The characterization of physical adsorption, acidity and crystallinity of five β -zeolites and the effect of acid sites of β -zeolites on deactivation, coke and aromatic yields.

| β -zeolite | | SAR 21 | SAR 25 | SAR 38 | SAR 75 | SAR 250 |
|----------------------------------------------------------------------------------------------------|-----------------------------|--------|--------|--------|--------|---------|
| BET (m ² /g) | | 657.2 | 619.6 | 671.6 | 615.1 | 598.9 |
| V _{pore} (mL/g) | | 0.87 | 1.04 | 0.35 | 1.01 | 0.44 |
| D _{pore} (Å) | | 53 | 67 | 21 | 66 | 30 |
| Crystallite size (nm) | | 7.3 | 6.9 | 8.2 | 7 | 7.9 |
| Acid sites by NH ₃ TPD (mmol/g) | | 1.7 | 1.24 | 0.98 | 0.53 | 0.2 |
| Brönsted acid (mmol/g) | | 0.33 | 0.28 | 0.37 | 0.18 | 0.1 |
| Lewis acid (mmol/g) | | 1.37 | 0.96 | 0.61 | 0.35 | 0.1 |
| Biomass-to-catalyst ratio | Intermediates breakthrough | 0.5 | 0.6 | 0.4 | 0.2 | 0.1 |
| | Primary vapors breakthrough | 1.1 | 1.1 | 0.8 | 0.6 | 0.5 |
| | Complete deactivation | 2 | 2 | 1.6 | 1.4 | 1.2 |
| Coke formed at the end of the experiment (g) | | 0.14 | 0.13 | 0.11 | 0.10 | 0.08 |
| Coke formed before primary breakthrough (g) | | 0.11 | 0.09 | 0.07 | 0.06 | 0.04 |
| Yield of coke at breakthrough of primary vapors (g coke/g biomass) | | 0.20 | 0.17 | 0.18 | 0.20 | 0.16 |
| Integration of one-ring aromatics before breakthrough of primary vapors ($\times 10^{10}$ counts) | | 13.7 | 11.9 | 8 | 7.7 | 3.8 |
| Yield of one-ring aromatics when primary vapors appear ($\times 10^{10}$ counts/g-pine) | | 1.5 | 1.2 | 1.1 | 1.9 | 0.9 |
| Coke formed per acid site before breakthrough of primary vapor (g coke/mmol) | | 0.13 | 0.15 | 0.15 | 0.23 | 0.40 |
| Yields of aromatics per site before breakthrough of primary vapor ($\times 10^{10}$ counts/mmol) | | 16 | 19 | 16 | 29 | 38 |
| Yield of aromatics per gram of coke formed ($\times 10^{10}$ counts/g coke) | | 125 | 127 | 111 | 128 | 95 |

Table 2. Analysis of products identified during vapor phase upgrading of pine pyrolysis products using SAR 25 β -zeolite with different biomass-to-catalyst ratios.

| MBMS | | | Compound Name | Compound Structure | GCMS | | |
|------|---------|---------|-----------------------|--------------------|----------------|----------------|----------------|
| m/z | B:C 0.5 | B:C 1.1 | | | B:C 0.125 | B:C 1.1 | B:C 2 |
| 18 | ✓ | ✓ | water | | - | - | - |
| 28 | ✓ | ✓ | carbon monoxide | $C=O$ | - | - | - |
| 42 | ✓ | ✓ | propene | | X | X | X |
| 44 | ✓ | ✓ | carbon dioxide | $O=C=O$ | X | X | X |
| | | | acetaldehyde | | - | X | X |
| 56 | ✓ | ✓ | 2-butene | | - | X | - |
| | | | 2-methylpropene | | X | X | - |
| | | | 2-propenal | | - | - | X |
| 58 | - | ✓ | acetone | | - | X | X |
| 60 | - | - | acetic acid | | - | - | X |
| 66 | ✓ | - | 1,3-cyclopentadiene | | - | - | X |
| 68 | - | ✓ | furan | | - | X | X |
| 70 | - | - | 2-propenal, 2-methyl | | - | - | X |
| 78 | ✓ | ✓ | benzene | | X | X | X |
| 82 | - | ✓ | furan, 2-methyl | | - | X | X |
| | | | furan, 3-methyl | | - | X | X |
| 92 | ✓ | ✓ | toluene | | X | X | X |
| 94 | - | ✓ | phenol | | - | X | X |
| 96 | - | ✓ | furan, 2,5-dimethyl | | - | X | X |
| | | | furfural | | - | - | X |
| 98 | - | ✓ | 1,2-cyclopentanedione | | - | - | X |
| 106 | ✓ | ✓ | ethyl benzene | | X | X | - |
| | | | p-xylene | | X ^a | X ^a | X ^a |
| | | | o-xylene | | X ^a | X ^a | - |
| 108 | - | ✓ | phenol, 2-methyl | | - | X | X |
| | | | phenol, 3-methyl | | - | X | X |

| | | | | | | | |
|-----|---|---|-----------------------------|-------------------------------------------------------------------------------------|----------------|----------------|----------------|
| 110 | - | ✓ | catechol |  | - | - | X |
| 116 | ✓ | ✓ | indene |  | - | X | X |
| 118 | - | ✓ | indane |  | - | X | - |
| | | | benzofuran |  | - | X | X |
| 120 | ✓ | ✓ | benzene, 1,3,5-trimethyl- |  | X ^a | X ^a | X ^a |
| | | | benzene, 1,2,3-trimethyl- |  | X ^a | X ^a | - |
| | | | benzene, 1-ethyl-3-methyl |  | X ^a | X ^a | - |
| | | | benzene, 1-ethyl-4-methyl |  | X ^a | X ^a | - |
| | | | benzene, 1-ethyl-2-methyl |  | X ^a | X ^a | - |
| 122 | - | ✓ | phenol, 2,5-dimethyl |  | - | - | X |
| | | | phenol, 2,4-dimethyl |  | - | - | X |
| 124 | - | ✓ | phenol, 2-methoxy |  | - | - | X |
| 128 | ✓ | ✓ | naphthalene |  | X | X | X |
| 132 | - | ✓ | benzofuran, 2-methyl |  | - | X | X |
| 134 | - | ✓ | 1,2,4,5-tetramethylbenzene |  | - | X ^a | - |
| 138 | - | ✓ | phenol, 2-methoxy-4-methyl- |  | - | - | X |
| 142 | ✓ | ✓ | naphthalene, 2-methyl- |  | X | X | - |
| | | | naphthalene, 1-methyl- |  | X ^a | X ^a | - |
| 150 | - | ✓ | 2-methoxy-4-vinylphenol |  | - | - | X |
| 152 | - | ✓ | phenol, 4-ethyl-2-methoxy- |  | - | - | X |
| 156 | ✓ | ✓ | naphthalene, 1,3-dimethyl- |  | X ^a | X ^a | X ^a |
| | | | naphthalene, 1,4-dimethyl- |  | X ^a | X ^a | - |
| | | | naphthalene, 1,7-dimethyl- |  | X ^a | X ^a | - |
| | | | naphthalene, 2,6-dimethyl- |  | X ^a | X ^a | - |

| | | | | | | | |
|-----|---|---|-----------------------------------------|-----------------------------------------------------------------------------------|---|---|---|
| 164 | - | - | phenol, 2-methoxy-5-(1-propenyl)-, (E)- |  | - | - | X |
| | | | phenol, 2-methoxy-4-(1-propenyl)- |  | - | - | X |
| | | | phenol, 2-methoxy-3-(2-propenyl)- |  | - | - | X |
| 170 | ✓ | - | naphthalene, 1,4,6-trimethyl- |  | - | X | - |
| | | | naphthalene, 2,3,6-trimethyl- |  | - | X | - |
| | | | naphthalene, 1,4,5-trimethyl- |  | - | X | - |
| 178 | ✓ | - | anthracene |  | - | X | - |
| 192 | ✓ | ✓ | anthracene, 2-methyl- |  | - | X | |
| 206 | ✓ | ✓ | anthracene, 1,3-dimethyl- |  | - | | |

✓ Peaks observed on the MBMS

X Assignments from NIST library

X^a Assignments from standards

This study investigates the role of β -zeolite acid site density on hydrocarbon and coke yields

